Shock-induced collapse of a cylindrical air cavity in water: a Free-Lagrange simulation

G.J. Ball[1], B.P. Howell[1], T.G. Leighton[2], M.J. Schofield[1]
[1]Department of Aeronautics and Astronautics, University of Southampton, SO17 1BJ, UK
[2]Institute of Sound and Vibration Research, University of Southampton, SO17 1BJ, UK

Abstract: A Free-Lagrange CFD code is used to simulate the collapse of a cylindrical air cavity in water by a $1.9GPa$ incident shock. This flow field models some aspects of sensitisation to shock-initiation of high explosives by cavities. The Lagrangian treatment allows the air/water interface to be tracked throughout the interaction. The incident shock is partially transmitted into the cavity, within which it experiences multiple reflections. The upstream cavity wall involutes to form a high-speed jet which, on impact with the far cavity wall, produces an intense blast wave. Sequential shock heating by the incident shock and the blast wave raises the air temperature to $\sim 15000K$.

Key words: Free-Lagrange Method, Bubble Collapse, Detonation Initiation, Cavitation

1. Introduction

This paper reports on a simulation of the response of a cylindrical air cavity to a shock of GPa order. Experimental investigations of collapses with such geometries have been undertaken for over a decade; Dear and Field(1988) achieved two-dimensional collapses of cavities shaped in gel, the geometry proving to be particularly useful for photographic studies of the bubble wall and interior. The impetus behind these studies was to understand the role of cavities in the initiation of reaction in commercial explosives. Such initiation is a thermal effect, and under conditions where bulk heating is insufficient to cause ignition, reaction might be initiated through hot-spots (Bowden and Yoffe (1958)). Adiabatic compression of gas pockets was identified as one amongst a range of mechanisms by which such hotspots might be produced (Field et al. (1982)). Chaudhri (1989) observed an initiation which was attributed to the impact of a high speed jet which developed within the collapsing cavity. That such jets could form had been suggested by Kornfeld and Suvorov (1944), and observed two decades later (Naudé and Ellis (1961)).

This paper is concerned with the thermal characteristics of cavities which involute to form jets. Bowden and Yoffe (1958) considered an adiabatic model of the compressed gas to be appropriate, given the speed of compression. Chaudhri and Field (1974) came to the same conclusion by observing the ignition of single crystals of silver or lead azide, or pentaerythritol tetranitrate, by attached bubbles. However, doubts about the ability of an adiabatically-heated gas to explain ignition in rapid collapses were raised (Starkenberg (1981)). Scales in both distance and time must be considered for heat conduction from the compressed gas to the liquid at the bubble wall (Chaudhri and Field (1974), Starkenberg (1981)), or to the small liquid droplets which are spalled off the wall into the gas pocket (Johansson (1958)), or to the liquid in the jet. Other possible causes of ignition were identified. Frey (1985) attributed temperature rise to the following sources: heating in the gas phase; hydrodynamic effects; the inviscid plastic work required to overcome the liquid yield strength; and viscoplastic work. Which dominates may depend on cavity size, liquid viscosity etc. (Mader and Kershner (1985, 1989)). Bourne and Field (1991, 1992) present results from the collapse of large (i.e. mm-order) air discs in a low-viscosity emulsion under high amplitude (GPa) shocks, and conclude that the two main causes of ignition are hydrodynamic heating in the region impacted by the jet, and adiabatic heating of the gas. When collapses occurred in a reactive emulsion, ignition occurred "firstly within the vapour contained within the cavity at the final moments of collapse, secondly in the material adjacent to the heated gas at the downstream cavity wall and thirdly, and principally, by hydrodynamic heating of material at the point of impact of the high-speed jet." Bourne and Field observed luminescence from the jet impact point and from the gas in the lobes generated as the jet bisects the air disc.

In the present work we have attempted to produce a numerical simulation of an experimental configuration used by Bourne and Field (1992) – a 6mm cylindrical air cavity in water impacted by a $1.9GPa$ shock – in order to gain further insight into the detailed mechanism of the shock/cavity interaction.

2. Numerical method

The simulation is performed using a recently developed Free-Lagrange CFD code *Vucalm* (Ball (1996)), which solves the two-dimensional unsteady Euler

equations on an unstructured Lagrangian grid using a Godunov-type method.

The working fluid is divided into discrete packets, between which mass exchange is forbidden. Flow variables are stored at a central "particle" within each packet which convects at the mass-mean velocity of the packet. The approximate locations of the packet boundaries are determined by constructing a Voronoi mesh, in which each particle is enclosed within a polygonal cell, forming a control volume for the time integration of the Euler equations. By definition, in a Voronoi mesh each cell encloses all points in the domain which are closer to the corresponding particle than to any other particle. The mesh is fully reconstructed after every five time steps to allow the grid connectivity to change naturally under the influence of shear; during intervening time steps the mesh vertices are convected at the local flow velocity – algebraic details are given in Ball (1996). For the present work, a mesh of approximately 5×10^4 cells has been used; the initial (unperturbed) mesh structure is square.

The equation of state for water is here approximated using the Tait equation:

$$p = B\left[\left(\frac{\rho}{\rho_R}\right)^{\gamma} - 1\right] \qquad (1)$$

where $\rho_R = 999.96 kg/m^3$ is a reference density at which $p = 0$, $B = 3.31 \times 10^8 Pa$, and $\gamma = 7$. The usual perfect gas equation of state is used in the air bubble. The simulation is inviscid, and no account is taken of real gas effects, heat transfer, inter-phase mass transfer or surface tension (but see below).

The Free-Lagrange methodology simplifies the treatment of multi-material problems in that each packet is assigned from the start of the simulation as either entirely air or entirely water; the type of fluid in a given packet never changes, and there are no mixed packets. Hence material interfaces always coincide with mesh cell boundaries, and are sharply resolved. An undesireable consequence of this is that material interfaces exhibit small-amplitude irregularities on the scale of the mesh cell size, which can trigger Richtmyer-Meshkov instability when strongly shocked. This problem is prevented in the present work by applying a simple interface smoothing routine which acts as a form of artificial surface tension – details will be reported elsewhere (Howell and Ball (1999)).

An additional consideration when using a Lagrangian mesh with an explicit scheme is that of timestep management. The maximum stable timestep for the method is limited by the usual CFL criterion. In flow regions subject to large compressions, such as the interior of the air cavity, the mesh itself becomes highly compacted, resulting in an uneconomically small maximum timestep. This problem is overcome in Vucalm using a "derefinement" algorithm which automatically merges adjacent pairs of cells in regions of excessive mesh density.

Three types of Riemann solver are used in this problem. At air/air cell interfaces an adaption of the HLLC approximate solver (Toro et al. (1994)) is used. At air/water interfaces an exact solver is employed (Flores and Holt (1981)). Finally, at water/water interfaces a two-shock variant of the Flores and Holt solver is used – this was found to be more numerically robust than the exact solver, which occasionally failed to converge in the highly sheared flow encountered after jet impact. Each of these solvers incorporates an explicit representation of the contact surface in the local Riemann problem. When implemented in the Lagrangian frame, where the cell boundary and the contact surface are coincident by definition, they give zero numerical diffusion at contact discontinuities and for convecting flow structure in general.

A piecewise-linear reconstruction of primitive variables (ρ,u,v,p) within grid cells is used to obtain nominal 2nd-order spatial accuracy; time integration is 1st-order. A slope limiter, based on the MUSCL approach, is used to prevent the creation of extrema in the local reconstruction, and hence avoid numerical oscillations at shocks.

The Vucalm code has been used previously to simulate blast refraction at contact surfaces between dissimilar gases (Ball and East (1996)) and at air/foam interfaces (Ball and East (1999)).

3. Problem specification

The problem studied in the present work is illustrated in Fig.1. A cylindrical air cavity, 6mm in diameter, is immersed in water at ISA sea-level conditions. A $1.9 GPa$ shock wave propagates through the water from left to right; all elapsed times are measured from the first shock/cavity contact. Only the upper half of

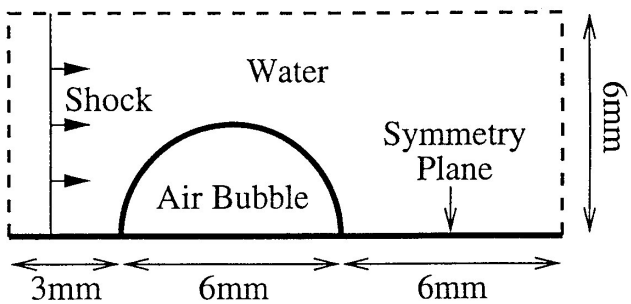

Figure 1. The Geometry of the problem.

the problem is simulated; the lower domain boundary

represents the plane of symmetry. Boundary conditions on the left boundary are initially fixed at post-shock values (inflow velocity $673m/s$) in order to generate the incoming shock wave, but, from t=0.5μs onwards, non-reflecting boundary conditions are applied in order to allow reflected waves to escape. The upper and right boundaries are non-reflecting at all times. Where inflow occurs, new particles are added automatically to maintain the Lagrangian mesh structure.

4. Results and discussion

At the initial conditions, the acoustic impedance of water is approximately 3600 times that of air. Consequently, when the incident water shock strikes the left bubble wall a relatively weak shock (approx $4MPa$) is transmitted into the air, and a strong expansion fan is produced in the water, running leftwards and upwards, while the bubble wall is deformed to the right – the situation at t=1.2μs is shown in Fig.2.

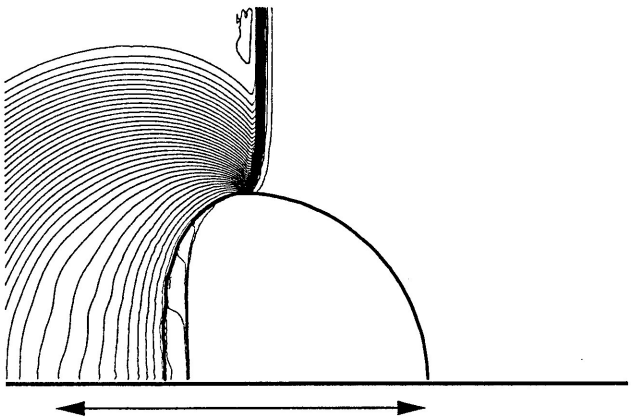

Figure 2. Shock/cavity interaction, t=1.2μs. Arrow indicates initial position and size of bubble; heavy line is bubble wall; contours are pressure:
$\Delta p = 10bar$ for $0 < p < 550bar$ (air only),
else $\Delta p = 500bar$

After 2.0μs (Fig.3) the incident water shock has traversed almost the full cavity width. The interaction between this shock and the expansion waves originating at the bubble surface has resulted in significant weakening and curvature of the shock. The air shock propagates more slowly, and has decoupled from the incident shock, while the left bubble wall has become involuted.

At t=2.5μs (Fig.4) a distinct water jet has formed running to the right along the symmetry axis. As the jet deforms the left bubble wall, compression waves are produced in the air, which progressively strengthen the air shock. By 2.8μs (Fig.5) this shock has formed an oblique reflection at the upper right bubble wall. Figures 6 to 8 show the evolution of the air shock/wall interaction; the incidence angle at the point of reflection increases with time due to the wall curvature, so that after about 40% of the shock length has undergone an oblique reflection, the remainder undergoes a near-normal reflection at around t=2.95μs.

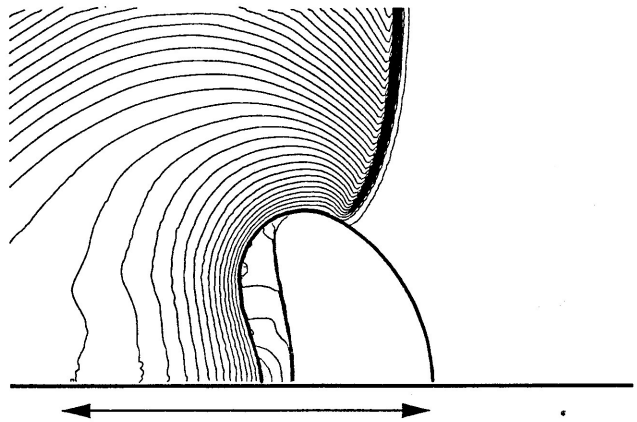

Figure 3. Shock/cavity interaction, t=2.0μs. Legend as Fig.2.

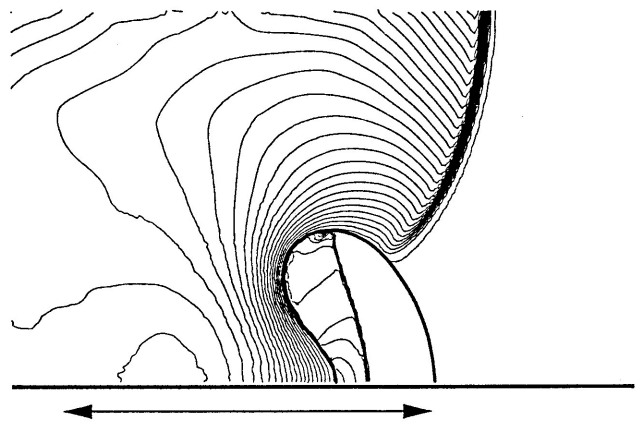

Figure 4. Shock/cavity interaction, t=2.5μs. Legend as Fig.2. Note water jet at left of bubble.

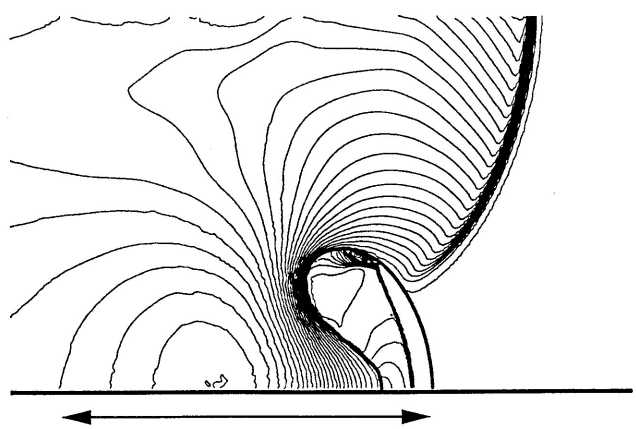

Figure 5. Shock/cavity interaction, t=2.8μs. Legend as Fig.2. Note oblique reflection of air shock at bubble wall.

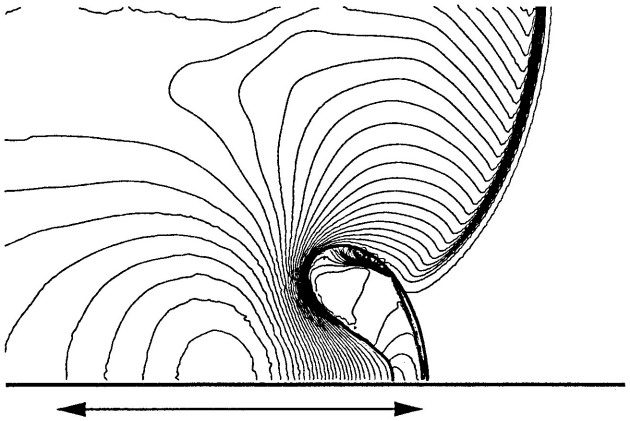

Figure 6. Shock/cavity interaction, t=2.9μs. Legend as Fig.2.

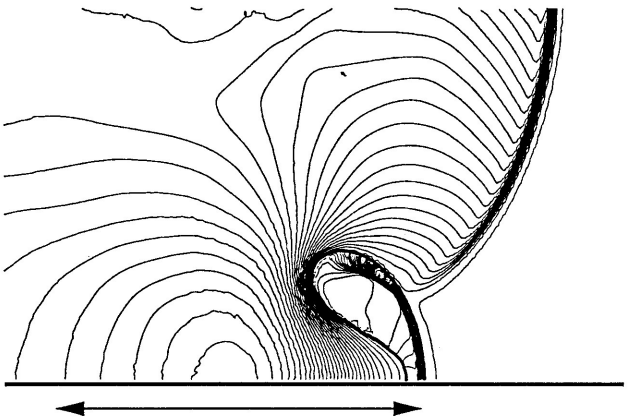

Figure 7. Shock/cavity interaction, t=3.0μs. Legend as Fig.2. Reflection of air shock below kink has occurred as normal reflection since t=2.9μs.

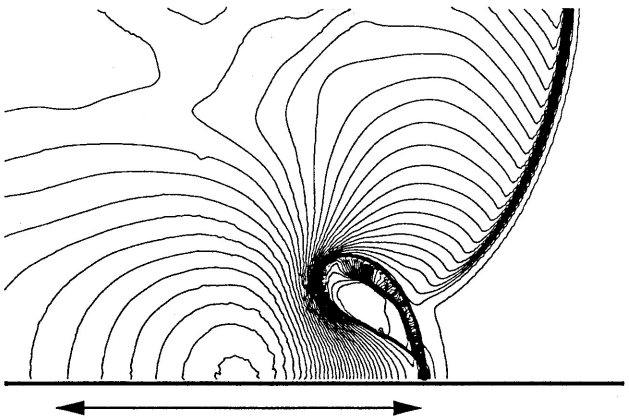

Figure 8. Shock/cavity interaction, t=3.1μs. Legend as Fig.2. Water jet impacts right bubble wall at approx. $2600 m/s$.

At t=3.1μs (Fig.8) the water jet reaches the right bubble wall, cutting the cavity in half. At this stage the peak water velocity in the jet is approximately $2600 m/s$. On impact, the jet produces an intense blast wave in the surrounding water with an initial peak overpressure exceeding $4.7 GPa$ (t=3.2μs, Fig.9). The air cavity resembles a tear-drop, and the air shock, now travelling to the left, has begun to interact with the lower left cavity wall, producing a Mach reflection. The subsequent evolution of the flow is shown in Figs.10 to 12. The airshock reaches the top of the cavity shortly after t=3.5μs. The predicted temperature in the shock-processed air varies with position over the range 5000K to $12000 K$ with pressures up to $0.3 GPa$. In view of the absence of heat transfer and real gas effects in this simulation, these temperature values should be regarded as only semi-quantitative, but nevertheless indicate that very intense heating of the gas phase does occur. The shape of the developing blast wave is worthy of note; because of the high water velocity in the jet fluid, the wave advances relatively slowly to the left below the bubble, so that the blast front is highly asymmetric. Below and to the right of the cavity, the interaction of the jet fluid with the surrounding low-momentum water produces a strong counter-clockwise vortex.

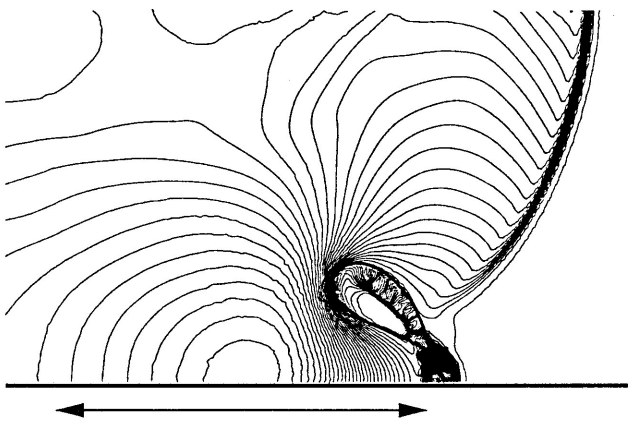

Figure 9. Shock/cavity interaction, t=3.2μs. Legend as Fig.2. Blast wave is formed; peak overpressure exceeds $4.7 GPa$.

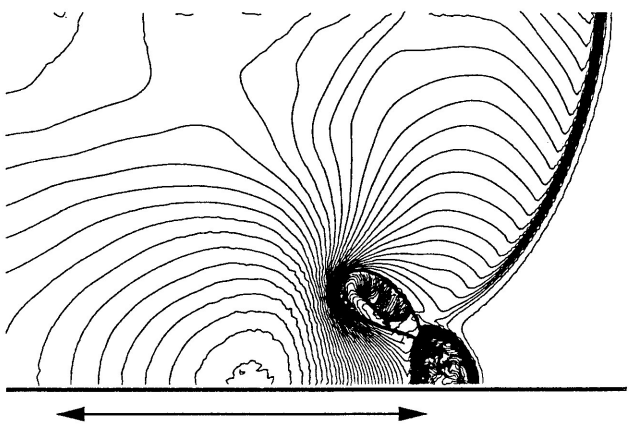

Figure 10. Shock/cavity interaction, t=3.3μs. Legend as Fig.2. Note Mach reflection of air shock.

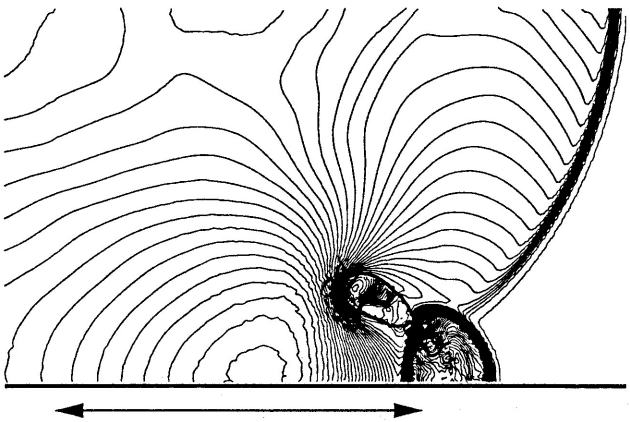

Figure 11. Shock/cavity interaction, t=3.4μs. Legend as Fig.2.

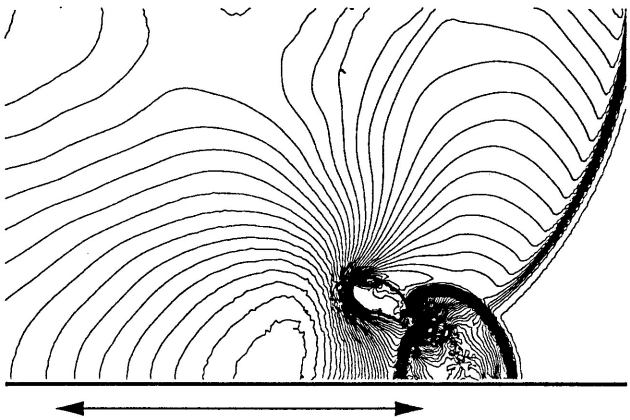

Figure 12. Shock/cavity interaction, t=3.5μs. Legend as Fig.2. Air shock reaches top of cavity; peak air temperature approx. 12000K

The final stages of the simulation are shown in Figs.13 to 15. At t=3.7μs a relatively weak compression wave propagates outwards from the cavity – this appears to be formed by partial transmission of the air shock into the water. It should be noted that the acoustic impedance of the air will have increased substantially due to increases in both density and wave speed in the air, so that the air/water mismatch decreases as the flow evolves, and hence air to water transmission becomes more efficient. At the same time, the cavity begins to be drawn into the vortex core due to baroclinicity. As a result of the cumulative effect of the derefinement algorithm, there are relatively few air particles remaining at this stage, so resolution of the cavity is poor, and geometric details of the cavity dynamics are therefore unreliable. By t=3.9μs the cavity has entered the vortex core, while the blast and compression waves are gradually merging. Finally, at t=4.3μs the air remains at the vortex core, which is now close to the right hand boundary of the original bubble, the blast and compression waves have almost merged, and the blast is more symmetrical. Conditions within the air are spatially almost uniform; the pressure is around 0.4GPa, while, as a result of additional heating on interaction with the blast wave, the temperature has risen to 15000K.

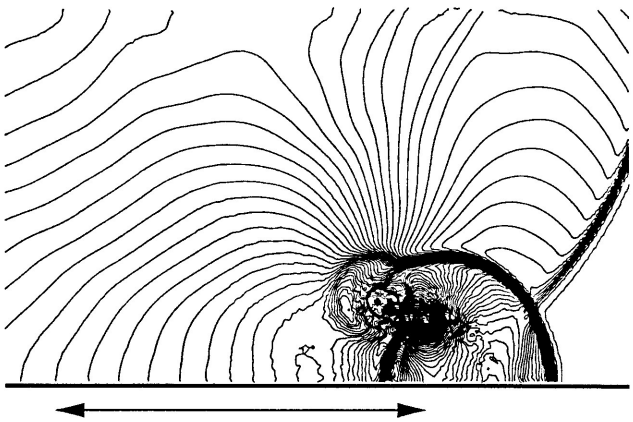

Figure 13. Shock/cavity interaction, t=3.7μs. Legend as Fig.2. Compression wave propagates from the cavity, which is baroclinically driven towards the vortex core.

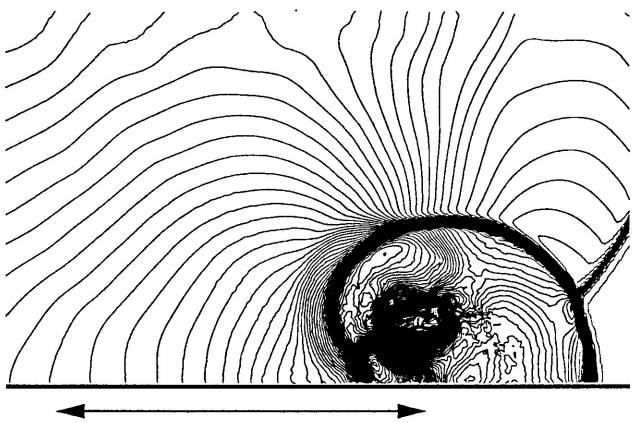

Figure 14. Shock/cavity interaction, t=3.9μs. Legend as Fig.2. Cavity has entered the vortex core.

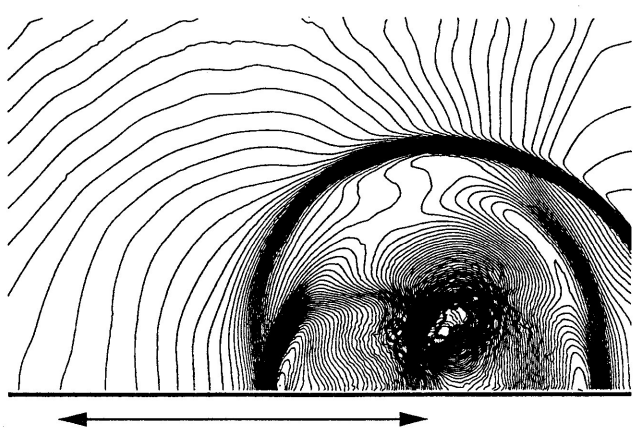

Figure 15. Shock/cavity interaction, t=4.3μs. Legend as Fig.2. Air in vortex core at 15000K and 0.4GPa

Where comparisons are possible, the results of this simulation broadly agree with the experimental results of Bourne and Field (1992) in terms of the geometry and temporal evolution of the interaction. In particular, they observed luminescence (their Fig 5(a)(iii)) at a time and position consistent with emission from the heated air trapped in the vortex core (Figs.14 and 15). In addition, the simulation predicts many details of the shock/cavity interaction which have not be determined experimentally due to the extreme practical difficulty of making measurements in this class of flow.

5. Conclusions

A Free-Lagrange code has been used to simulate the interaction between a strong underwater shock wave and a cylindrical air cavity. The interaction is shown to be physically complex. Air within the cavity is heated and compressed by a sequence of mutiply-reflected shock waves, attaining a final temperature of the order of $15000K$. Under the flow conditions represented here, shock heating would appear to play a key role in generating the experimentally-observed luminescence, and clearly provides a credible mechanism for detonation initiation in high explosives containing cavities.

Acknowledgement. The authors are grateful to Prof. R Hillier for his valuable advice on the use of the Tait equation.

References

Ball GJ (1996) A Free-Lagrange method for unsteady compressible flow: simulation of a confined cylindrical blast wave. Shock Waves 5:311–325

Ball GJ, East RA (1996) Refraction of a blast wave propagating parallel to a contact discontinuity: a Free-Lagrange numerical simulation. Proceedings of the 20th International Symposium on Shock Waves: 557–562

Ball GJ, East RA (1999) Shock and blast attenuation by aqueous foam barriers: influences of barrier geometry. Shock waves 9:37–47

Bourne NK, Field JE (1991) Bubble collapse and the initiation of explosion. Proc. Roy. Soc. Lond. A435:423–435

Bourne NK, Field JE (1992) Shock-induced collapse of single cavities in liquids. Journal of Fluid Mechanics 244:225–240

Bowden FP, and Yoffe AD, (1958) Fast reaction in solids. London: Butterworths.

Chaudhri MM, Field JE, (1974) The role of rapidly compressed gas pockets in the initiation of condensed explosives. Proc. Roy. Soc.Lond A340:113–128

Chaudhri MM, (1989) The initiation of fast decomposition in solid explosives by fracture, plastic flow, friction and collapsig voids. Proc. Ninth Symposium (International) on Detonation, Portland, Oregon, pp. 857–868

Dear JP, Field JE, (1988) A study of the collapse of arrays of cavities. J. Fluid Mech. 190:409–424

Field JE, Swallowe GM, and Heavens SN, (1982) Ignition mechanisms of explosives during mechanical deformation. Proc. Roy. Soc. Lond., A383, 231–244.

Flores J, Holt M (1981) Glimm's method applied to underwater explosions. Jornal of Computational Physics 44:377–387

Frey RB, (1985) Cavity collapse in energetic materials. Eighth Symposium (International) on Detonation, pp.68–80

Howell BP, Ball GJ (1999) Damping of mesh-induced errors in Free-Lagrange simulations of Richtmyer-Meshkov instability. Proceedings of the 22nd International Symposium on Shock Waves

Johansson CH, (1958) The initiation of liquid explosives by shock and the importance of liquid break up. Proc. R. Soc. Lond. A246:160–167

Kornfeld M, Suvorov L, (1944) On the destructive action of cavitation. J Appl. Phys. 15:495–506

Mader CL, Kershner JD, (1985) The three-dimensional hydrodynamic hot-spot model. In Proc. Eighth Symposium (International) on Detonation, pp.42–52

Mader CL, Kershner JD, (1989) The heterogeneous explosive reaction zone. In Proc. Ninth Symposium (International) on Detonation, pp.693–700

Naudé CF, Ellis AT, (1961) On the mechanism of cavitation damage by nonhemispherical cavities collapsing in contact with a solid boundary. Trans. ASME D: J. Basic Engng. 83, 648–656

Starkenberg J, (1981) Ignition of solid high eplosive by the rapid compression of an adjacent gas layer. Proc. Seventh Symposium (International) on Detonation, pp.3–16

Toro EF, Spruce M, Speares W (1994) Restoration of the contact surface in the HLL Riemann solver. Shock Waves 4:25–34